

Higher Martian atmospheric temperatures at all altitudes increase the D/H fractionation factor and water loss

E. M. Cangi^{1,2}, M. S. Chaffin¹, J. Deighan¹

¹Laboratory for Atmospheric and Space Physics

²University of Colorado Boulder

¹3665 Discovery Dr, Boulder, CO 80303

²Boulder, CO

Key Points:

- The fractionation factor f is most strongly controlled by non-thermal escape of atomic deuterium (D).
- Larger f correlates minimally with higher atmospheric temperature at the surface, but strongly with exobase and tropopause temperatures.
- Using our results for f , we calculate total water lost from Mars to be between 66-122 m GEL, which is likely a lower bound.

Abstract

Much of the water that once flowed on the surface of Mars was lost to space long ago, and the total amount lost remains unknown. Clues to the amount lost can be found by studying hydrogen (H) and its isotope deuterium (D), which are produced when atmospheric water molecules H_2O and HDO dissociate. The difference in escape efficiencies of H and D (which leads to an enhanced D/H ratio) is referred to as the fractionation factor f . Both the D/H ratio and f are necessary to estimate water loss; thus, if we can constrain the range of f and understand what controls it, we will be able to estimate water loss more accurately. In this study, we use a 1D photochemical model of the neutral Martian atmosphere to determine how f depends on assumed temperature and water vapor profiles. We find that the exobase temperature most strongly controls the value of f for thermal escape processes. When we include estimates of non-thermal escape from other studies, we find that the tropopause temperature is also important. Overall, for the standard Martian atmosphere, $f = 0.002$ for thermal escape, and $f = 0.06$ for thermal + non-thermal escape. We estimate that Mars has lost at minimum 66-122 m GEL of water. Importantly, our results demonstrate that the value of f depends critically on non-thermal escape of D, and that modeling studies that include D/H fractionation must model both neutral and ion processes throughout the atmosphere.

Plain Language Summary

Mars used to have lots of water, but has lost it over time. When water molecules break apart in the atmosphere, they release hydrogen (H) and its heavier twin deuterium (D), which escape to space at different rates, removing water from Mars. The escape efficiency of D compared to H is called the fractionation factor f . The goal of this study is two-fold: to understand how f varies with different atmospheric conditions and the processes that control it, and to use that information to estimate water loss from Mars. To do this, we model the Martian atmosphere to test how different atmospheric temperatures and water vapor content affect f . We find that the most important thing affecting f is loss of D via processes involving interaction with planetary ions or the solar wind, rather than loss of D that is hot enough to exceed escape velocity. This implies future studies must include ion chemistry to accurately calculate f . We also find that generally, temperatures above 100 km strongly affect the value of f . Using these results, we calculate that Mars has lost enough water to cover the whole planet in a layer between 66-122 m deep.

1 The D/H Fractionation Factor and Loss of Martian Water to Space

The surface of Mars is marked with ample evidence of its wetter past. Today, water on Mars exists only in the polar caps, subsurface ice, and atmosphere, but geomorphological and geochemical evidence points to significant alteration of the surface by liquid water. The presence of compounds like jarosite and hematite indicate past pooling and evaporation (Squyres et al., 2004; Klingelhöfer et al., 2004), while substantial evidence of hydrated silicates supports the theory that ancient river deltas, lake beds, catastrophic flood channels, and dendritic valley networks were formed by water (M. H. Carr & Head, 2010; Ehlmann & Edwards, 2014, and references therein). Because the contemporary Martian climate cannot support liquid water on the surface, Mars must have once had a thicker and warmer atmosphere. The Mars science community generally agrees that the atmosphere has escaped over time, with a significant amount in the form of thermal escape of H, in which a fraction of H atoms are hot enough that their velocity exceeds the escape velocity. Because H is primarily found in water on Mars, this has effectively desiccated the planet (Jakosky et al., 2018).

A significant indicator of this loss of water to space is the elevated D (deuterium, ^2H or D) to H (hydrogen, ^1H) ratio, which we will abbreviate as R_{dh} . Because water (ei-

ther as H₂O or HDO) is the primary reservoir of both H and D, when we talk about the D/H ratio, we are thus usually referring to D/H measured in water:

$$R_{dh} = \frac{\text{D in HDO}}{\text{H from HDO} + \text{H from H}_2\text{O}} = \frac{[\text{HDO}]}{[\text{HDO}] + 2[\text{H}_2\text{O}]} \approx \frac{[\text{HDO}]}{2[\text{H}_2\text{O}]} \quad (1)$$

Here, $[X]$ represents a molecule's abundance; H sourced from HDO is negligible compared to H sourced from H₂O. This ratio evolves according to differential escape of D and H; D, being twice as massive as H, is less likely to escape. This difference can be characterized as a relative efficiency, the fractionation factor f :

$$f = \frac{\phi_{\text{D}}/\phi_{\text{H}}}{[\text{HDO}]_s/2[\text{H}_2\text{O}]_s} = \frac{\phi_{\text{D}}/\phi_{\text{H}}}{R_{dh,s}} \quad (2)$$

where ϕ represents fluxes to space, and the s subscript specifies the near-surface atmospheric reservoir, which approximates the total amount in the atmosphere. As it represents efficiency of D escape, f takes on values between 0 and 1. When f is 0, D is completely retained on the planet, and cumulative water loss must have been lower than for $f \neq 0$. When $f = 1$, the *ratio* of escaping to retained atoms is the same for both D and H, and there is no mass effect on the escape rates. In this scenario, no amount of escape is sufficient to change the D/H ratio in any species. In practice, f is somewhere in between these extremes.

Over geologic time, this fractionation manifests as an enhancement of the D/H ratio compared to the Earth ratio of 1.6×10^{-4} (Yung et al., 1988), called SMOW (for the measured source, Standard Mean Ocean Water). A planet's D/H ratio is often quoted as a multiple of the Earth value. At present, multiple measurements put the global mean R_{dh} on Mars between 4 and $6 \times$ SMOW (Owen et al., 1988; Bjoraker et al., 1989; V. Krasnopolsky et al., 1997; Encrenaz et al., 2018; Vandaele et al., 2019), with some variations occurring on local spatial and temporal scales (Villanueva et al., 2015; Clarke et al., 2017; Encrenaz et al., 2018; Clarke et al., 2019; Villanueva et al., 2019). This is most commonly interpreted as evidence for significant escape to space of H.

To estimate the integrated amount of water lost, one can use current estimates of the Martian water inventory, R_{dh} , and f with the Rayleigh distillation equation for H (Yung & DeMore, 1998):

$$R_{dh}(t) = R_{dh}(t=0) \left(\frac{[\text{H}](0)}{[\text{H}](t)} \right)^{1-f}, \quad (3)$$

where $t = 0$ can be arbitrarily chosen. Because we use R_{dh} and because water is the primary reservoir of H on Mars, $[\text{H}]$ is commonly replaced with total water W ($W = [\text{H}_2\text{O}] + [\text{HDO}]$). Then $W(0)$, the total water on Mars at some point in the past $t = 0$, is the sum of the water budget at time t and the total water lost: $W(0) = W(t) + W_{\text{textlost}}$. Substituting W for $[\text{H}]$ and rearranging equation 3, we obtain an expression for water lost from Mars:

$$W_{\text{lost}} = W(t) \left(\left(\frac{R_{dh}(t)}{R_{dh}(0)} \right)^{1/(1-f)} - 1 \right) \quad (4)$$

Most of the inputs to Equation 4 are well-described. The current D/H ratio of exchangeable water (the atmosphere, seasonal polar caps, ground ice, and water adsorbed in the regolith), $R_{dh}(t)$, is $4\text{--}6 \times$ SMOW as mentioned (we use 5.5 in this study). $R_{dh}(0)$ is usually taken to be that at Mars' formation, when it would have been similar to the

Earth’s D/H ratio (Geiss & Reeves, 1981); R_{dh} at other points in time can be obtained from meteorite samples (Usui et al., 2012, e.g.) or in-situ analysis (Mahaffy et al., 2015, e.g.). The current water inventory in exchangeable reservoirs, $W(t)$, is estimated to be between 20-30 m GEL (global equivalent layer), the depth of water if the entire exchangeable inventory were rained onto the surface (Zuber et al., 1998; Plaut et al., 2007; Lاسue et al., 2013; Villanueva et al., 2015; M. Carr & Head, 2019).

Prior studies estimated the fractionation factor f , but its range of values under all plausible scenarios has been largely unexplored. Yung et al. (1988) used a 1D photochemical model to calculate a first value of $f = 0.32$ which has been frequently referenced in the years since. They explored the effects of certain chemical reactions on f , but did not test other parameters. V. A. Krasnopolsky and Mumma (1998) obtained $f = 0.02$ by combining Hubble Space Telescope observations with a radiative transfer and 1D photochemical model. Later, V. Krasnopolsky (2000) followed up with another study that tested the effects of two different models of eddy diffusion, finding values of $f = 0.135$ and $f = 0.016$. Two years later, V. A. Krasnopolsky (2002) found 3 values for f , depending on whether the solar cycle was at minimum ($f = 0.055$), maximum ($f = 0.167$), or mean ($f = 0.082$), represented in the model by variation of the exobase temperature and non-thermal escape flux. Our goal is to advance this body of work by performing the first systematic parameter-space study of the fractionation factor with respect to the assumed atmospheric temperature and water vapor profiles.

2 Building Our 1D Photochemical Model

To best capture the mean behavior of the Martian atmosphere over long time scales, we use a 1D photochemical model, extended from the original developed by Chaffin et al. (2017) to include D chemistry. The model uses standard photochemical techniques described in other studies (V. Krasnopolsky, 1993; Nair et al., 1994; Chaffin et al., 2017), with the addition of the D-bearing species D, HD, HDO, OD, HDO₂, DO₂, and DOCO. The chemical reactions for D-bearing species came from several sources, including past papers (Yung et al., 1988; Yung et al., 1989; Cazaux et al., 2010; Deighan, 2012), NASA publications (Sander et al., 2011), and online databases (Manion et al., 2015; Wakelam & Gratier, 2019; McElroy et al., 2013). The full list of chemical reactions and reaction rates, as well as details on implemented photochemical cross sections (Barfield et al., 1972; Nee & Lee, 1984; Cheng et al., 1999, 2004) and diffusion coefficients (Banks & Kockarts, 1973), is given in the Supporting Information. Photodissociation is driven by solar UV irradiation data from SORCE/SOLSTICE and TIMED/SEE (Woods et al., 2019), appropriate for solar mean conditions and scaled to Mars’ orbit. For our primary input, we construct temperature and water vapor profiles designed to represent end-member states of the atmosphere, such that we fully constrain the range of plausible fractionation factor values.

A run of the model consists of the following steps: (1) loading the temperature and water vapor profiles, (2) establishing an initial condition of species number densities, (3) establishing boundary conditions (Table S3), and (4) stepping forward over 10 million years of simulation time until the atmosphere reaches chemical equilibrium, which is achieved when the combined escape flux of atomic H and D ($\phi_H + \phi_D$) is twice that of the escape flux of atomic O (ϕ_O). (This stoichiometric balance is required because H and D are primarily sourced from water.) The model output comprises species number densities by altitude. By multiplying the H- and D-bearing atomic and molecular species densities by their thermal effusion velocities (Hunten, 1973), we can calculate ϕ_H and ϕ_D :

$$\phi_H = n_H v_H + 2n_{H_2} v_{H_2} + n_{HD} v_{HD} \quad (5)$$

$$\phi_D = n_D v_D + n_{HD} v_{HD} \quad (6)$$

These fluxes are then used to calculate f according to equation 2.

A limitation of our model is that we do not include a full ionosphere. Instead, we approximate it by including a static profile of CO_2^+ (Matta et al., 2013), enabling the primary H-producing ion reaction in the Martian atmosphere; a similar tactic was used by Yung et al. (1988). Without a full ionosphere, we are not able to model non-thermal escape of H or D, as most non-thermal processes depend on ions. In an effort to estimate the relative importance of non-thermal processes to the fractionation factor, we estimate non-thermal effusion velocities for our model conditions, scaled from V. A. Krasnopolsky (2002), described further in Section 3.

2.1 Reproductions of Past Studies

Before proceeding with our study, we attempted to reproduce the results by Yung et al. (1988) and V. A. Krasnopolsky (2002). Their original results and our reproductions are shown in Figure S3. We achieved very good agreement with the results by Yung et al. (1988), finding $f = 0.26$ versus their $f = 0.32$. The small difference is due to the only two differences between the model by Yung et al. (1988) and ours. First, Yung et al. (1988) manually fix their photodissociation rates, whereas our model calculates them. Second, they adopt the water profile used by Liu and Donahue (1976), fixing it below 80 km and allowing it to vary above, whereas we fix it throughout the atmosphere. Our results for f were consistent with V. A. Krasnopolsky (2002) for solar maximum, but comparatively low for solar mean and minimum. We expect that this is because their model includes an ionosphere, allowing them to model non-thermal escape. To account for this, we added their results for non-thermal escape of D to our results for thermal escape, resulting in a slight overestimate instead of an underestimate. This change was a first hint at the importance of non-thermal escape to f . The remaining discrepancy is due to other significant model differences, irreconcilable without rewriting our model; for example, their model atmosphere has its lower bound at 80 km, while ours is at the surface. This difference in model extent means that our two models also have significant differences in temperature structure and boundary conditions.

2.2 Model input: Temperature and Water Vapor Profiles

Our temperature and water vapor vertical profiles remain fixed for the duration of a simulation. This allows us to examine the mean behavior of the atmosphere over long time scales.

2.2.1 Temperature Profiles

The piecewise temperature profile is modeled with equation 7. The general form is based on measurements by the Viking orbiters (Seiff, 1982), and similar models have been used in other studies (e.g. McElroy, Kong, & Yung, 1977; Nair et al., 1994; V. A. Krasnopolsky, 2010). In the lower atmosphere, the temperature decreases with altitude according to the dry adiabatic lapse rate Γ . At the tropopause (altitude z_t), temperature reaches a minimum and remains isothermal in the mesosphere. Above the mesopause (120 km), upper atmospheric density is low enough that UV heating is efficient, causing the temperature to increase rapidly with altitude.

$$T = \begin{cases} T_{\text{exo}} - (T_{\text{exo}} - T_{\text{tropo}}) \exp\left(-\frac{(z-120)^2}{8T_{\text{exo}}}\right) & z > 120 \text{ km} \\ T_{\text{tropo}} & z_t < z < 120 \text{ km} \\ T_{\text{surf}} + \Gamma z & z < z_t \end{cases} \quad (7)$$

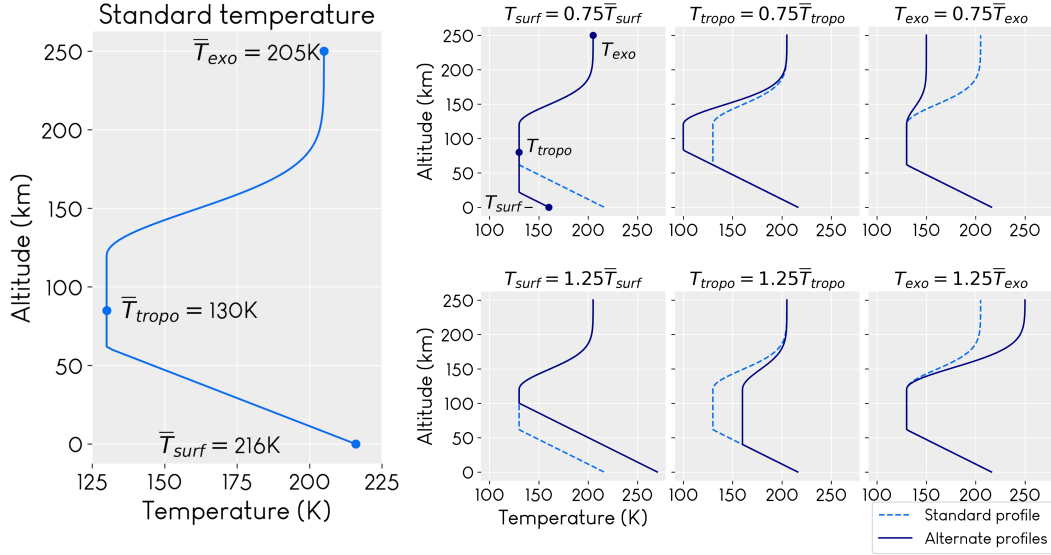


Figure 1. a) Our standard temperature profile used in the model, and b) alternate temperature profiles representing plausible climate extrema due to obliquity variations. Profiles are created by modifying the standard temperatures \bar{T}_{surf} , \bar{T}_{tropo} , or \bar{T}_{exo} by $\pm 25\%$. We do not consider effects of CO_2 condensation for cold temperatures, although this would be important in real atmospheres. These profiles, along with the standard profile, are used to obtain the results in Figure 4. Table S4 gives specific values for T_{surf} , T_{tropo} , T_{exo} .

We constrain this modeled profile with the temperatures at the surface (T_{surf}), tropopause (T_{tropo}), and exobase (T_{exo}). Constraining the temperature at these three points requires either Γ or z_t to vary; if they are both fixed, the profile will be over-constrained and discontinuous. We allow z_t to vary as it does in reality (e.g., Forget et al., 2009); exactly what sets its altitude is less well defined than the dynamics of gas and dust, on which Γ depends. We use $\Gamma = -1.4$ K/km, which is slightly lower than the standard dry adiabatic lapse rate due to warming effects from suspended dust (Zahnle et al., 2008).

For the first part of the study, we constructed a standard temperature profile representing current conditions on Mars, as well as 6 alternate profiles intended to represent plausible climate extrema driven by changing planetary obliquity throughout the last ~ 10 million years of Mars' history, the maximum time over which obliquity evolution can be analytically predicted. (On longer time scales, the obliquity evolves chaotically, making precise definition of climate parameters impossible (Laskar et al., 2004).) We used the Mars Climate Database (MCD) (Millour & Forget, 2018) to obtain values for T_{surf} ($z = 0$), T_{tropo} ($z = 100$ km), and T_{exo} ($z = 250$ km) for different times of sol (local times 03:00, 09:00, 15:00, 21:00), Mars latitude ($90^\circ N$, $45^\circ N$, 0° , $45^\circ S$, $90^\circ S$), and L_s (90° and 270°), then compared the mean temperatures across each of these parameters with data from multiple missions to ensure consistency. The surface temperature was compared with the Curiosity Rover (Vasavada et al., 2016; Audouard et al., 2016; Savijärvi et al., 2019), Mars Global Surveyor Thermal Emission Spectrometer (TES) (Smith, 2004), and the Spirit/Opportunity Rovers' Mini-TES (Smith et al., 2006); the exobase temperature was compared with MAVEN data from multiple instruments (Bougher et al., 2017; Stone et al., 2018; Thiemann et al., 2018). The mean temperatures formed the standard profile, shown in Figure 1a. Figure 1b shows the 6 alternate profiles, in which we varied one of T_{surf} , T_{tropo} , or T_{exo} by $\pm 25\%$ of the standard value. This variation covers most values observed by current missions, as well as temperatures calculated (Wordsworth

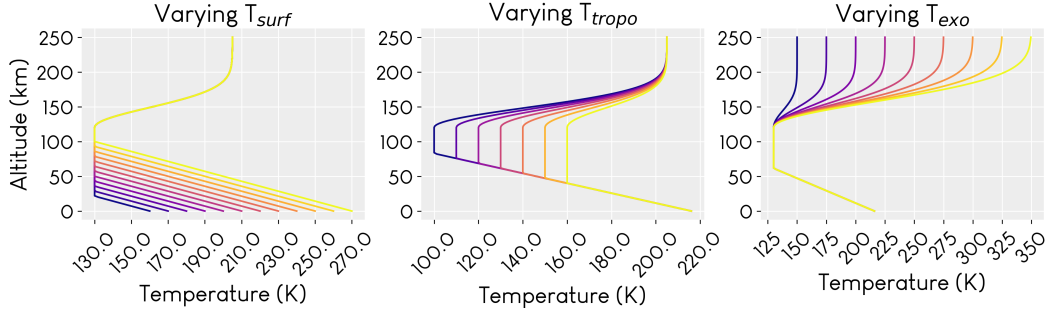


Figure 2. The full range of temperature profiles tested. Each panel represents a set of profiles in which one of the specifiable temperatures was varied. Results from the simulations using these profiles are shown in Figure 5. Each color represents a different profile.

et al., 2015) for obliquities of $\sim 25\text{--}45^\circ$ predicted for the last 10 million years (Laskar et al., 2004). A table with the control temperatures for each profile is available in the Supporting Information. Together, the standard and alternate temperature profiles represent end-member cases for the Martian atmosphere.

In addition to these select profiles, we also created a larger set of temperature profiles with finer variation in each of T_{surf} , T_{tropo} , or T_{exo} to examine the details of how each parameter affects f . This set of temperature profiles is shown in Figure 2.

2.2.2 Water Profiles

H_2O and HDO profiles used in the model are shown in Figure 3. We require that the profiles have total water content ($\text{H}_2\text{O} + \text{HDO}$) equal to 1, 10, 25, 50, or 100 $\text{pr } \mu\text{m}$ (precipitable micrometers), with H_2O making up most of the share. Higher concentrations of water vapor would require a supersaturated atmosphere; while there is observational evidence of supersaturation at upper altitudes in specific cases (Maltagliati, 2011; Fedorova et al., 2020), our model does not include it. We use the 10 $\text{pr } \mu\text{m}$ profile to represent the long-term standard atmosphere, a value in agreement with observations (Lammer et al., 2003; Smith, 2004), although more recent observations (Heavens et al., 2018; Vandaele et al., 2019) and modeling (Shaposhnikov et al., 2019) suggest that local water vapor concentrations can reach higher values, up to 150 $\text{pr } \mu\text{m}$, on very short timescales, particularly during dust storms. We assume that the lower atmosphere is well-mixed, such that the water vapor mixing ratio is constant. At the hygropause, usually between 25 and 50 km (V. Krasnopolsky, 2000; Heavens et al., 2018), water begins to condense, and its mixing ratio follows the saturation vapor pressure curve until it becomes negligible in the upper atmosphere (Heavens et al., 2018). Although HDO preferentially condenses compared to H_2O (Montmessin et al., 2005), it never approaches saturation in our model atmosphere, allowing us to use the same empirical saturation vapor pressure equation (Marti & Mauersberger, 1993) for both H_2O and HDO. This is helpful, as no empirical equation for HDO exists, and the enthalpies of HDO under Mars-like conditions are very sparsely studied.

Although observations (Villanueva et al., 2015) and modeling (Fouchet & Lellouch, 1999; Bertaux & Montmessin, 2001) have shown that atmospheric D/H varies between 1-10 \times SMOW depending on the species it is measured in, altitude, and latitude/longitude, we tested these variations and determined that they had no effect on our results. We therefore multiply the initial profiles of H-bearing species by the D/H ratio of $5.5\times$ SMOW to create the D-bearing profiles. The number densities of H_2O and HDO remain fixed

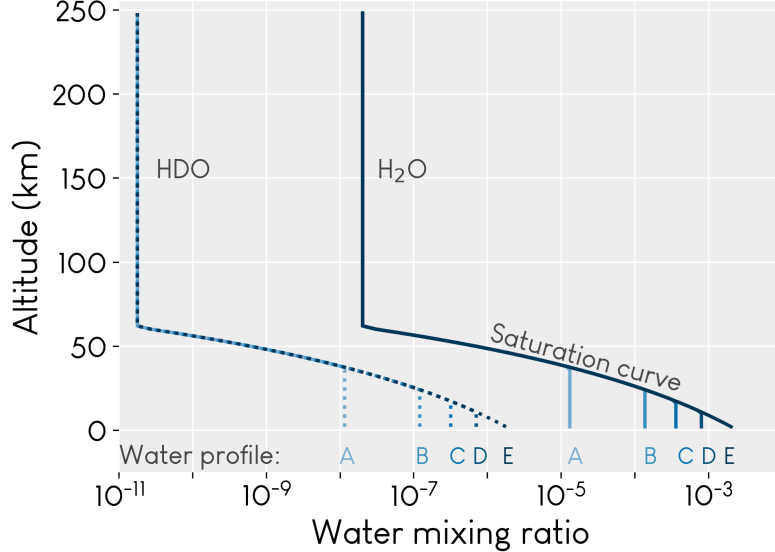


Figure 3. Water vapor profiles used in our model. A single profile, e.g. A, comprises both H_2O (solid lines) and HDO (dotted). Profiles are constrained by requiring that $[\text{H}_2\text{O}] + [\text{HDO}] = 1 \text{ pr } \mu\text{m}$ (profile A), 10 (B), 25 (C), 50 (D), or 100 (E) and that the HDO profile is equal to $5.5 \times \text{SMOW} \times$ the H_2O profile. Profiles differ in the well-mixed lower atmosphere and are the same once they reach the saturation vapor pressure curve. Water vapor in the mesosphere and upper atmosphere is negligible on average over long time scales, like those we model, although it may change on short time scales (see text). Profile B (10 $\text{pr } \mu\text{m}$) is used for our standard atmosphere.

during the simulation to represent the standard water abundance, though they are used to calculate chemical reaction rates.

3 Results: Temperature Variations and Non-thermal Escape Critical to Understanding the Fractionation Factor

Figure 4 shows the range of the fractionation factor as a function of each temperature and water vapor parameter, using the temperature profiles in Figure 1 and the water vapor profiles in Figure 3. Results for the broad range of temperatures shown in Figure 2 are discussed in Section 3.1.

For thermal escape only, we find that f is 1-3 orders of magnitude lower than the original value by Yung et al. (1988). The primary reason for this difference is the exobase temperature (they use 364 K, while we use a maximum of 250 K, which is more consistent with modern measurements). Other minor differences are as described in Section 2.1. Details of the dependence of f on each parameter are discussed in sections 3.1 and 3.2.

Because our model does not include an ionosphere, we do not model the effects of non-thermal escape processes (e.g. sputtering, photochemical escape), and only model thermal escape. This makes it difficult to compare with other studies which do include non-thermal escape (e.g. V. A. Krasnopolsky, 2002). In order to compare with that study, we must estimate v_{nt} , the non-thermal escape velocity, which is not part of our model. To do so, we calculated the ratio of thermal to non-thermal effusion velocities ($r = v_t/v_{nt}$) for H, H_2 , D, and HD in the model used by V. A. Krasnopolsky (2002). We then divided our v_t by the ratio r to get an estimate of non-thermal effusion velocities v_{nt} at the tem-

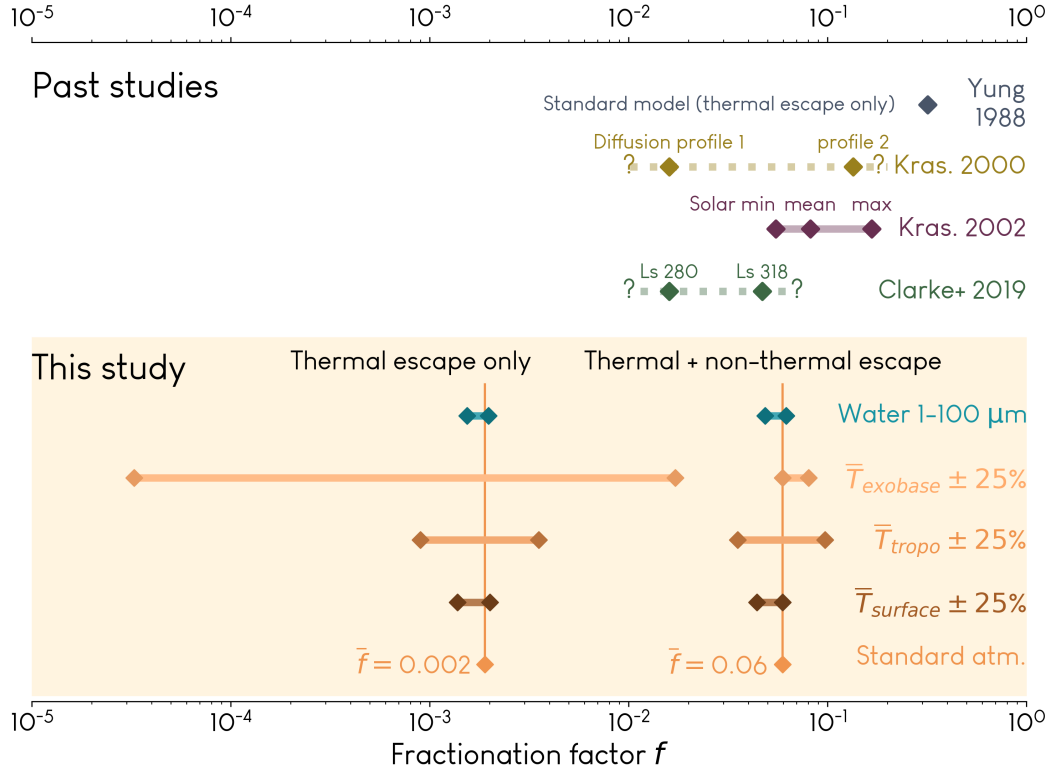


Figure 4. Results for the fractionation factor from this study (lower panel) and in past studies (upper panel). Bars represent the approximate range. Dotted lines with question marks indicate a study where the cases chosen did not necessarily represent end-member cases, so the true range is uncertain. Details of the dependence of f on temperatures and water vapor (orange and blue bars in lower panel) are shown in Figures 5 and 7. A numerical table of our results is available in Table S5.

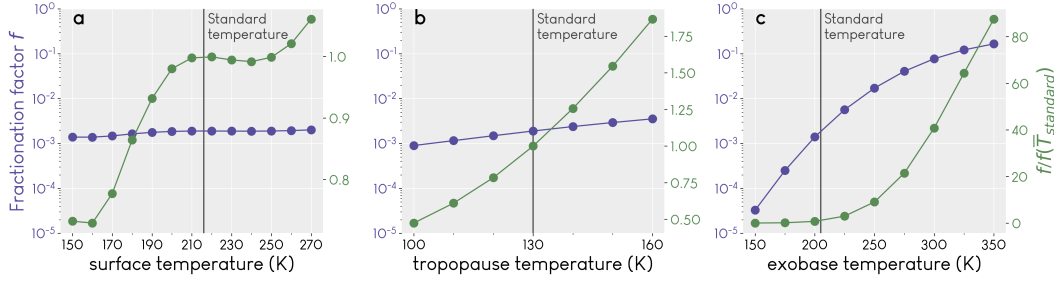


Figure 5. Dependence of the fractionation factor f on changes in the surface, tropopause, and exobase temperatures. The standard value of each is marked by a black vertical line. The left (purple) axis shows the value of f , while the right (green) axis shows the relative change of f with respect to that calculated for the standard temperature.

temperatures modeled by V. A. Krasnopolsky (2002): 200 K, 270 K, and 350 K. We extrapolated this estimate down to 150 K, the lowest temperature in our model, by fitting a 2nd order polynomial to the estimates for v_{nt} , allowing us to estimate the role that non-thermal escape plays in setting f for the temperature profiles shown in Figure 1. Though the estimation method is imperfect, it provides a rough estimation while avoiding unphysical velocity values at low temperatures, and gives values of f that are consistent with V. Krasnopolsky (2000) and V. A. Krasnopolsky (2002), as well as more recent observations using MAVEN/IUVS (Clarke et al., 2019). Notably, our highest value of f is approximately a factor of 3 larger than the lowest, in agreement with V. A. Krasnopolsky (2002). In future work beyond the scope of this paper, we plan to directly model non-thermal contributions, enabling a better model comparison.

3.1 Fractionation Factor for Thermal Escape Strongly Controlled by Exobase Temperature

Figure 5 shows in detail how f varies with each temperature parameter for the modeled thermal escape only. This approach allows us to focus on what we can learn about f from our model, and refrain from drawing any strong conclusions about specific effects introduced by non-thermal escape before we can fully model it. The results show that an increase in temperature in any part of the atmosphere leads to an increase of f (less fractionation). The effect is small when the temperature increase occurs in the lower atmosphere, and dramatic when the change occurs at the exobase. Understanding this behavior requires examining the temperature-dependent behavior of H, D, H₂, and HD abundances and the escape fluxes ϕ_D and ϕ_H . This information is shown in Figure 6, where we plot these values for each simulation, normalized to the simulation with the standard atmosphere.

As a function of both surface and tropopause temperature, ϕ_D most closely tracks the abundance of atomic D at the exobase. Per equation 2, f depends directly on ϕ_D , inversely on ϕ_H , and inversely on $R_{dh,s}$. $R_{dh,s}$ is constant, and any reduction of ϕ_H is offset by an increase in ϕ_D because stoichiometric balance requires that $\phi_H + \phi_D = 2\phi_O$. This change is many orders of magnitude smaller than ϕ_H and thus not visible in Figure 6, but comparable to ϕ_D , making it easily visible. The increase of f with T_{tropo} is thus primarily because the higher temperatures in the mesosphere and thermosphere enable greater transport of D upwards. This response is possible because D is not diffusion-limited. Moderate increases in ϕ_D are a by-product of this effect (see Figure S6), as the escaping population is proportional to the upper-atmospheric abundance of D. Transport into the mesosphere may also be slightly enhanced by increased T_{surf} , but the main

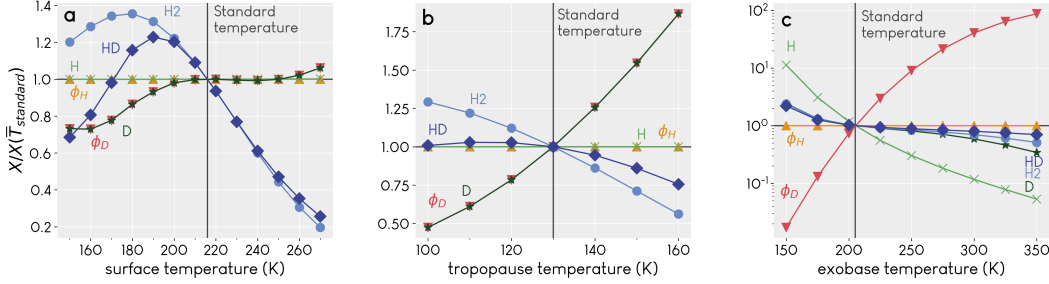


Figure 6. Change in exobase abundances of H- and D-bearing species or escape fluxes (ϕ) as a function of temperature for thermal escape only. ϕ_H and ϕ_D are calculated as in equations 5 and 6. In panels a and b, ϕ_D (and thus f in Figure 5a and b) closely tracks the abundance of atomic D. In panel c, changes in the abundance of H, D, H₂ and HD are caused by both escape to space and supply by diffusion from below. D is not diffusion limited, so ϕ_D responds more strongly to temperature forcing than H. Note the linear y-scale in panels a and b and the log scale in panel c. In all panels, ϕ_H is on the order of $\sim 10^8 \text{ cm}^{-2}\text{s}^{-1}$, but differences between simulations are on the order of 10, making the relative variation of $\phi_H \cong 1$.

role of T_{surf} is to drive the chemical reaction rates in the dense lower atmosphere, where they dominate over transport in controlling species abundances.

In contrast, the exobase temperature T_{exo} has a far greater effect on the value of f , with values ranging from 10^{-5} to 10^{-1} . This is unsurprising, as f directly depends on ϕ_D . Because thermal populations are assumed to be Maxwellian, we take the velocity in equations 5 and 6 to be the effusion velocity, which depends directly on T_{exo} . As T_{exo} rises, the warmer thermosphere to enable enhanced vertical transport of D. Escape of D is enhanced enough that ϕ_D no longer closely tracks the abundance of atomic D. To compensate for the increased loss of D while maintaining stoichiometric balance, ϕ_H must decrease by a negligible amount (see Figure S7).

3.2 Fractionation Factor Depends Weakly on Water Vapor Column Abundance

The fractionation factor as a function of total water vapor is shown in Figure 7a, and the comparison of abundances and fluxes of H- and D-bearing species in Figure 7b. As in the previous section, the increase of f with additional water vapor is correlated with an increased abundance of D at the exobase, but also HD. The total water vapor has little effect on f , likely because the absolute abundance of water changes neither the D/H ratio in water or the processes by which it is fractionated. The small variation with respect to water vapor thus reflects the influence of minor differences in H₂O and HDO chemical and photochemical reactions. In order to more fully characterize the effects of water vapor on f , the model will have to be modified to allow variable water vapor profiles.

3.3 Mapping Fractionation Factor Results to Integrated Water Loss

We can determine the magnitude of water loss on Mars by using our results for f as input to Equation 4. These results are shown in Figure 8. In order to use Equation 4 to plot past water loss, we must set values for the current water inventory $W(t)$, the current D/H ratio $R_{dh}(t)$, and the ancient Martian D/H ratio, $R_{dh}(0)$.

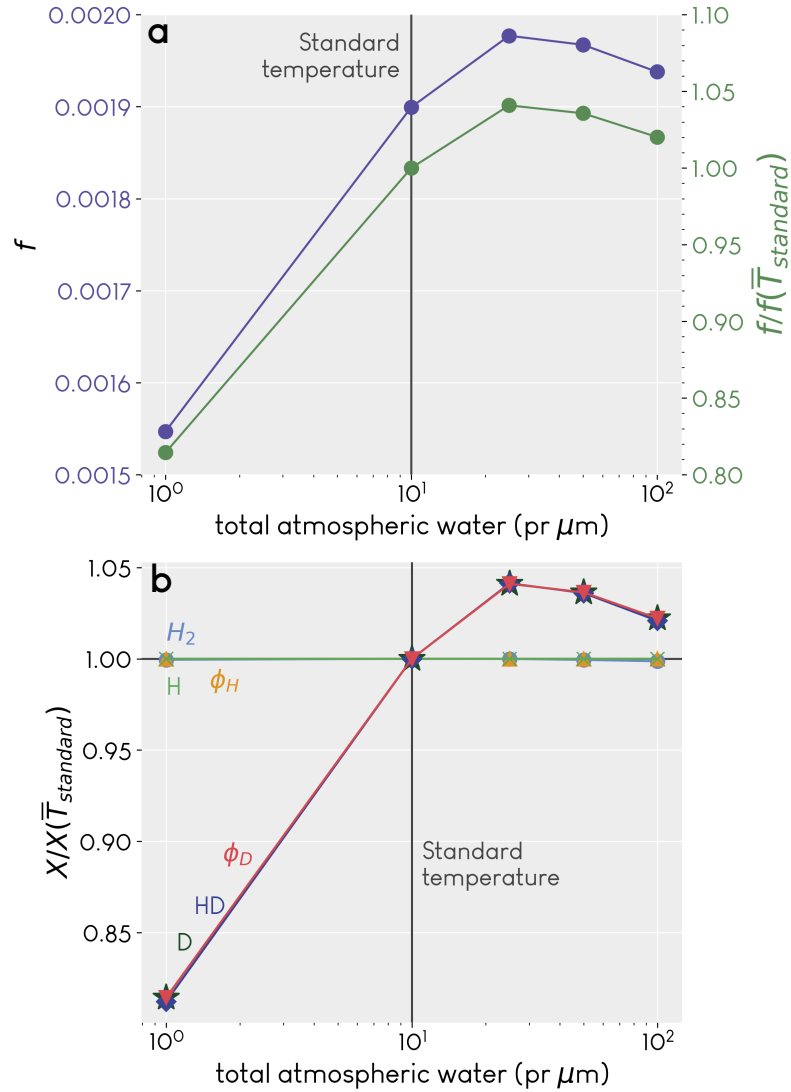


Figure 7. a) Fractionation factor f as a function of water vapor column abundance, shown for concentrations of 1, 10, 25, 50, and 100 pr μm , for thermal escape only. b) Same as Figure 6, but as a function of water vapor. Here, ϕ_D and f track the abundances of both D and HD.

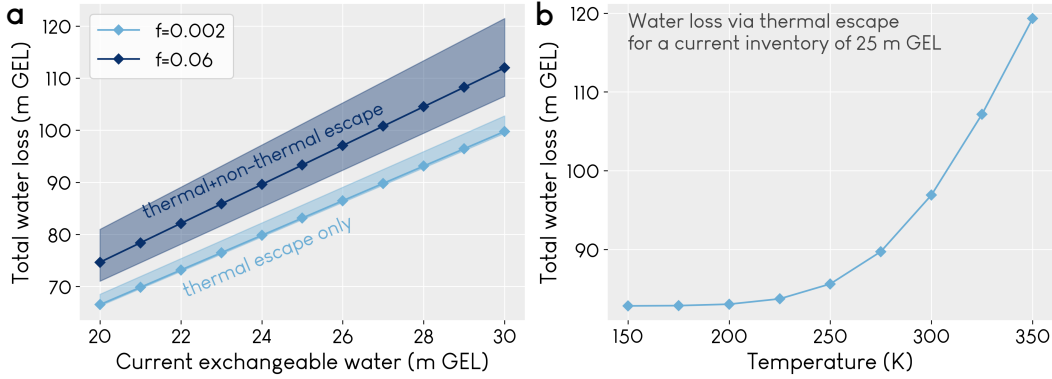


Figure 8. Water lost from Mars a) as a function of the current exchangeable water budget and the fractionation factor for the standard atmosphere ($f=0.002$ for thermal escape and $f=0.06$ for thermal and non-thermal together). The shaded regions represent the extrema of water loss, calculated for the extrema of f of each escape type from our results. The lower bound for thermal escape is close to that of the standard case because water loss is insensitive to f for $f<0.01$. b) as a function of exobase temperature and f for that temperature as calculated in the model. Water loss is calculated using Equation 4. Equation parameters are described in Section 3.3. Because we do not model non-thermal escape, the top line in panel a includes an approximation of the effect of non-thermal escape as described in the main text.

For $W(t)$, we use the aforementioned range 20-30 m GEL for the current exchangeable water budget of Mars. Exchangeable water is water that is able to move between surface deposits and the atmosphere; its D/H ratio increases due to escape to space. Non-exchangeable water, being unaffected by escape to space, would have its original D/H value.

For $R_{dh}(0)$, we follow Kurokawa et al. (2014) and Villanueva et al. (2015) and use $1.275 \times \text{SMOW}$, in agreement with the measurement of D/H in the 4.5 billion year old melt inclusions in the Martian meteorite Yamato 980459 (Usui et al., 2012). Finally, we use $5.5 \times \text{SMOW}$ for $R_{dh}(t)$.

Using these values, we calculate the cumulative water lost to be between about 66 and 122 m GEL, depending on escape type and value of f . We compare these results with other estimates in the literature in the next section.

4 Discussion

Because f depends directly on the escape fluxes ϕ_D and ϕ_H , it is reasonable that the exobase temperature would most strongly affect f for thermal escape. Disturbances in the lower atmosphere that may otherwise affect f will be reduced in amplitude by the time they propagate to the upper atmosphere. A larger f at higher exobase temperatures also makes sense in the context of past work; the Mariner missions measured the exobase temperature to be 350 ± 100 K (Anderson & Hord, 1971), and Yung et al. (1988) used $T_{\text{exo}} = 364$ K to obtain $f = 0.32$ for thermal escape only. However, these original Mariner measurements were highly uncertain; more recent data (discussed previously) indicate that T_{exo} during solar mean and minimum is cold enough that f for thermal escape is substantially smaller, and that non-thermal escape of D is critical to an accurate calculation of f .

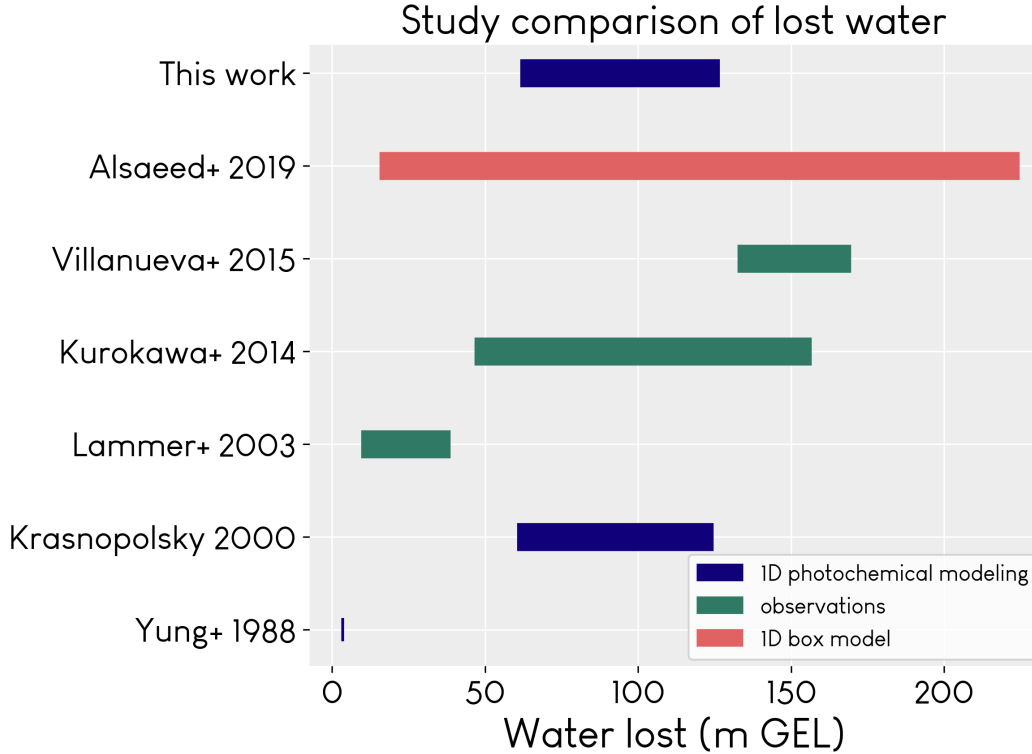


Figure 9. Estimates of water lost from Mars by various studies.

The importance of T_{tropo} is also worth some discussion. In Figure 4, T_{tropo} appears to be the parameter with the greatest control over f for thermal + non-thermal escape together. It should be noted, however, that our estimates of non-thermal escape are approximate and extrapolated below 200 K, as described in Section 3. For the simulations that varied T_{surf} or T_{tropo} , each estimation of non-thermal escape was made assuming a constant value of T_{exo} (205 K). On the other hand, different values of T_{exo} were necessarily used in the simulations which tested the effects of varying it. This means that $f_{\text{thermal+nonthermal}}$ and f_{thermal} as a function of T_{tropo} appear to differ by a constant, whereas $f_{\text{thermal+nonthermal}}$ as a function of T_{exo} may be artificially large at temperatures below 200 K (see Figure S5). Despite these uncertainties, T_{tropo} is still important to the value of f , as increased T_{tropo} also increases the temperature of the thermosphere, enabling greater upward transport and contributing to overall escape (see Figure S6).

The relationship of ϕ_{D} from thermal escape to the abundances of atomic D and HD is not immediately obvious. In Figure 6a and b, ϕ_{D} most closely tracks the abundance of atomic D at the exobase because it is much more abundant than HD. In all of the simulations represented in these panels, the exobase temperature is 205 K, a value too low for escape of HD to contribute significantly to D loss. Only at high exobase temperatures (Figure 6c) or high concentrations of water (Figure 7b) does ϕ_{D} appear to track the HD abundance, indicating HD is abundant enough to contribute more to D loss. In general, in Figures 6 and 7b, an increase in ϕ_{D} is correlated with an increase in the abundance of D, except when T_{exo} increases and escape is dramatically enhanced. More abundant deuterium means more deuterium available to escape; in most cases, loss of deuterium (hydrogen) via D (H) dominates, but at high exobase temperatures, loss via the molecular form HD (H_2) can reach higher values, up to 5% (20%), as shown in Figure S4.

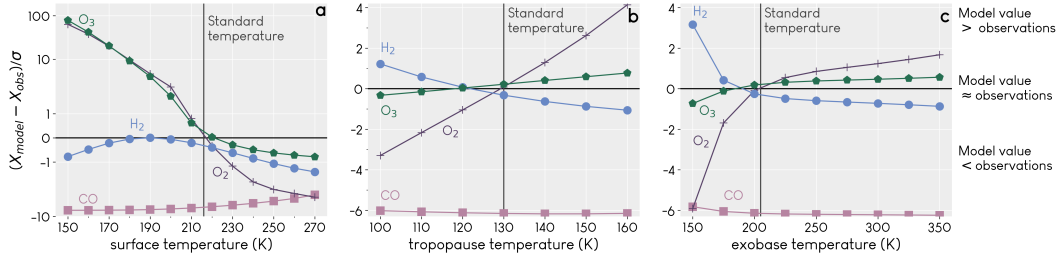


Figure 10. Comparison of model output values to measured values as a means of determining appropriateness of our temperature assumptions. See text for measurement citations. O_3 is measured in $\mu\text{m-atm}$. O_2 and CO are measured as the mixing ratio at the surface. H_2 is measured with the total abundance in ppm in the lower atmosphere (0-80 km). The y-axis is the difference between model output and measurement, weighted by the uncertainty in the measurement; the closer a point is to the 0 line, the more similar the model output and measurement.

A comparison of our results for water loss to those of other similar studies is shown in Figure 9. Overall, our results agree reasonably well with these other studies. Our results are a little lower than those by Villanueva et al. (2015), who assume a higher atmospheric D/H ratio ($7\text{-}8 \times \text{SMOW}$), and a little higher than Lammer et al. (2003), who assume a higher D/H ratio for early Mars ($1.2\text{-}2.6 \times \text{SMOW}$) and a lower estimate of the current exchangeable water (3.3-15 m GEL). The original study by Yung et al. (1988) is an outlier in this case because they were attempting to determine both the current water inventory and the amount lost, and did not have the benefit of the many Mars missions and observations that we have today. The recent work by Alsaeed and Jakosky (2019) is unique compared to the other studies in this figure in that they allow water to be added to the atmosphere via volcanic outgassing, so that their results represent a large possible solution space and are less directly comparable than the other studies.

Our results for water loss also bring up an important point with regard to escape rates. It is common when estimating water loss on Mars to assume that the escape fluxes ϕ_{H} and ϕ_{D} are constant and that the water inventory decreases linearly with time. This is an often necessary but imperfect assumption due to the many unknowns involved, including historical rates of atmospheric escape and their evolution in light of Mars’ chaotically evolving obliquity. Assuming linear loss with time (and neglecting ϕ_{D} , which is far slower than ϕ_{H}) gives $\phi_{\text{H}} = W_{\text{lost}}/t$, where t is the time over which the water has been lost. Using our results for water loss, even the smallest amount lost (about 60 m GEL) requires an escape rate of $\sim 3 \times 10^9 \text{ cm}^{-2} \text{ s}^{-1}$, an order of magnitude higher than what we currently observe for escape rates of H from Mars (Jakosky et al., 2018). This is an indication that escape rates were likely higher in the past due to a variety of factors, especially in the context of a more UV-active young sun (Jakosky et al., 2018), or that surface interactions play a larger role that has been previously explored—e.g., with regard to oxygen deposition (Zahnle et al., 2008)—but not yet fully quantified.

As a way to gain insight about our results, we compared the concentrations of a few molecular species in our model with available measurements (Figures 10 and 11). The measurements we used were the inferred lower atmospheric abundance of $\text{H}_2 = 15 \pm 5 \text{ ppm}$ (V. A. Krasnopolsky & Feldman, 2001); a global mean O_3 abundance of $1.2 \mu\text{m-atm}$, extracted from maps by Clancy et al. (2016); and mixing ratios for O_2 and CO at the surface equal to $(5.8 \pm 0.8) \times 10^{-4}$ and $(1.61 \pm 0.09) \times 10^{-3}$ (Trainer et al., 2019). These comparisons indicate the model conditions which may be more similar or dissimilar to the current state of Mars. As one example, model results that used a particularly low temperature as input (for example, models with $T_{\text{surf}} < 190$ or $T_{\text{exo}} < 175$) di-

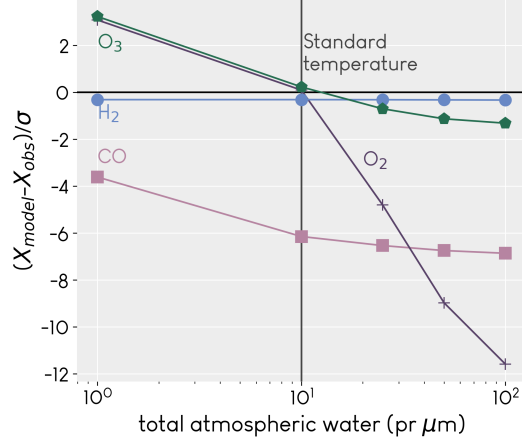


Figure 11. The same as Figure 10, but for model runs where we varied the water vapor content of the atmosphere.

verge greatly from measurements of all molecular species. These model results thus represent a significant perturbation to the photochemical system as compared to modern Mars. It is also important to note that O_3 and O_2 are related, as O_3 is created and destroyed via interactions between O_2 and O . CO sticks out as an obvious problem; this is not surprising, as many photochemical models also have difficulty in reproducing the observed values (V. A. Krasnopolsky, 2010). Some models come close (e.g. Zahnle et al. (2008)), usually only when another parameter changes significantly. Our model also underestimates CO , reaffirming the ongoing need for study in this area. Apart from CO , the difference between our model and measurements is mostly small, indicating that the standard atmosphere we chose was reasonable.

Our results represent a peri-modern global scenario; f has likely changed over time in ways that our model does not account for. In this work, we consider only the exchangeable reservoirs of water on Mars without including any type of surface deposition, which comprises multiple processes with potentially different fractionation factors. Fractionation may also vary on seasonal timescales, especially around the poles, as HDO preferentially condenses and may also have a different sublimation rate compared to H_2O . It has certainly varied over geological time scales. We run the model for 10 million years to equilibrium, though it would not necessarily have been in equilibrium throughout its 4.5 billion year history. This also means that atmospheric escape rates would not have been constant in time, although we assume them to be because their time evolution is unknown. Mars’ chaotically evolving obliquity on time scales greater than 10 million years is a major reason for this lack of a definitive paleo-climate timeline. Characterization of escape rates through time is therefore a critical, but daunting, subject for future modeling efforts. On early Mars, the more UV-active young sun would have enhanced non-thermal escape rates (Jakosky et al., 2018), allowing f to grow larger due to the enhancement of ϕ_{D} . This is allowed even in long-term chemical equilibrium; when no D is present, $\phi_{\text{H}} = 2\phi_{\text{O}}$, but when D is present, the requirement instead becomes $\phi_{\text{H}} + \phi_{\text{D}} = 2\phi_{\text{O}}$. For all these reasons, we expect that our results for water loss are a lower bound.

5 Conclusions

Our results in Figure 4 and Table S5 show that if only thermal escape is considered, the exobase temperature has the strongest effect on the fractionation factor, whereas when non-thermal escape is included, the temperatures of the tropopause and exobase

become comparably important (given the uncertainty in our non-thermal escape estimation). While the exobase and upper atmosphere have been the focus of many recent studies, the Martian mesosphere is less well-studied, but is worthy of future modeling and observational efforts. The tropopause temperature affects mesospheric chemistry, which is especially important considering the seasonal transport of water to these altitudes (Chaffin et al., 2017; Heavens et al., 2018; Shaposhnikov et al., 2019; Fedorova et al., 2020). Because T_{tropo} is the minimum temperature in the atmosphere, a larger value also implies a warmer thermosphere (see Figure 2), which may contribute to enhanced transport, especially above the homopause.

Our results also show how important non-thermal escape is to accurately calculate f . For thermal escape processes only, D is almost completely retained on Mars compared to H. This is especially true near solar maximum, when most atmospheric loss occurs as thermal escape of H. During solar mean and minimum, however, thermal escape of both D and H is low enough that the non-thermal loss of D and HD becomes much more significant (V. A. Krasnopolsky & Mumma, 1998; Gacesa et al., 2012). Figure 4 shows that including non-thermal escape increases f by an order of magnitude or more for all atmospheric conditions. Studies of only thermal escape are therefore not likely to provide a reasonable estimate of f . We therefore advise that future modeling studies that calculate f should include non-thermal escape; this will also enable better comparison with recent observationally-derived values of f (e.g. Clarke et al., 2019).

In this study, we have neglected interaction with the planetary surface, which is certainly important due to the unknown D/H of surface ice and polar caps and fractionating effects on sublimation and deposition. Future work to understand the fractionation factor and atmospheric escape will need to link cross-disciplinary knowledge of surface and atmospheric processes. The history of water on Mars cannot be fully understood by only considering one or the other; they are inextricably linked. A more thorough understanding of exchange between different water reservoirs on and under the surface and in the atmosphere, as well as the variables affecting all types of atmospheric escape and water loss, will be instrumental in forming a more complete picture of the fractionation factor, and by extension water loss, on Mars.

Acknowledgments

This work was supported by MDAP grant #NNX14AM20G. Additionally, this material is based upon work supported by the National Science Foundation Graduate Research Fellowship Program under Grant No. DGE 1650115. Any opinions, findings, and conclusions or recommendations expressed in this material are those of the author(s) and do not necessarily reflect the views of the National Science Foundation. The authors would like to thank B. Jakosky, N. Alsaeed, L. Wernicke, and D. Brain for ongoing collaboration, feedback, and support. The model, input information, and generated output can be found on Zenodo (Cangi et al., 2020).

References

- Alsaeed, N. R., & Jakosky, B. M. (2019). Mars Water and D/H Evolution From 3.3 Ga to Present. *Journal of Geophysical Research: Planets*, *124*. doi: 10.1029/2019JE006066
- Anderson, D. E., & Hord, C. W. (1971). Mariner 6 and 7 Ultraviolet Spectrometer Experiment: Analysis of hydrogen Lyman-alpha data. *Journal of Geophysical Research*, *76*. doi: 10.1029/ja076i028p06666
- Audouard, J., Piqueux, S., Poulet, F., Vincendon, M., Gondet, B., & Rogers, D. A. (2016). Analysis of Curiosity Surface Temperature Data. In *47th lunar and planetary sciences conference*.
- Banks, P. M., & Kockarts, G. (1973). *Aeronomy*. Academic Press, Inc.

- Barfield, W., Koontz, G., & Huebner, W. (1972). Fits to new calculations of photoionization cross sections for low-z elements. *Journal of Quantitative Spectroscopy and Radiative Transfer*, *12*. doi: 10.1016/0022-4073(72)90043-X
- Bertaux, J., & Montmessin, F. (2001). Isotopic fractionation through water vapor condensation: The Deuteropause, a cold trap for deuterium in the atmosphere of Mars. *Journal of Geophysical Research-Planets*, *106*. doi: 10.1029/2000JE001358
- Bjoraker, G. L., Mumma, M. J., & Larson, H. P. (1989). Isotopic Abundance Ratios for Hydrogen and Oxygen in the Martian Atmosphere. In *AAS/Division for Planetary Sciences 21st annual meeting*.
- Bougher, S. W., Roeten, K. J., Olsen, K., Mahaffy, P. R., Benna, M., Elrod, M., ... Jakosky, B. M. (2017). The structure and variability of Mars dayside thermosphere from MAVEN NGIMS and IUVS measurements: Seasonal and solar activity trends in scale heights and temperatures. *Journal of Geophysical Research: Space Physics*, *122*. doi: 10.1002/2016JA023454
- Cangi, E., Chaffin, M. S., & Deighan, J. (2020, October). *emcangi/dh_fractionation Mars D Photochemistry*. Retrieved from <http://doi.org/10.5281/zenodo.4110723> doi: 10.5281/zenodo.4110723
- Carr, M., & Head, J. (2019). Mars: Formation and fate of a frozen Hesperian ocean. *Icarus*, *319*. doi: 10.1016/j.icarus.2018.08.021
- Carr, M. H., & Head, J. W. (2010). Geologic history of Mars. *Earth and Planetary Science Letters*, *294*. doi: 10.1016/j.epsl.2009.06.042
- Cazaux, S., Cobut, V., Marseille, M., Spaans, M., & Caselli, P. (2010). Water formation on bare grains: When the chemistry on dust impacts interstellar gas. *Astronomy & Astrophysics*, *522*. doi: 10.1051/0004-6361/201014026
- Chaffin, M. S., Deighan, J., Schneider, N. M., & Stewart, A. I. F. (2017). Elevated atmospheric escape of atomic hydrogen from Mars induced by high-altitude water. *Nature Geoscience*, *10*. doi: 10.1038/ngeo2887
- Cheng, B. M., Chew, E. P., Liu, C. P., et al. (1999). Photo-induced fractionation of water isotopomers in the Martian atmosphere. *Geophysical Research Letters*, *26*. doi: 10.1029/1999GL008367
- Cheng, B. M., Chung, C. Y., Bahou, M., Lee, Y. P., Lee, L. C., Van Harreveld, R., & Van Hemert, M. C. (2004). Quantitative spectroscopic and theoretical study of the optical absorption spectra of H₂O, HOD, and D₂O in the 125-145 nm region. *Journal of Chemical Physics*, *120*. doi: 10.1063/1.1630304
- Clancy, R. T., Wolff, M. J., Lefèvre, F., Cantor, B. A., Malin, M. C., & Smith, M. D. (2016). Daily global mapping of Mars ozone column abundances with MARCI UV band imaging. *Icarus*, *266*. doi: 10.1016/j.icarus.2015.11.016
- Clarke, J. T., Mayyasi, M., Bhattacharyya, D., et al. (2017). Variability of D and H in the Martian upper atmosphere observed with the MAVEN IUVS echelle channel. *Journal of Geophysical Research: Space Physics*, *122*. doi: 10.1002/2016JA023479
- Clarke, J. T., Mayyasi, M., Bhattacharyya, D., Schneider, N., Chaufray, J.-Y., Bertaux, J.-L., ... Yelle, R. (2019, Sept). The D/H Ratio in the Martian Upper Atmosphere. In *European Planetary Science Congress and AAS/Division for Planetary Sciences 2019 joint meeting*. (EPSC-DPS2019-868-1)
- Deighan, J. (2012). *The effect of an ozone layer on ancient mars* (Doctoral dissertation, University of Virginia). Retrieved from <http://libra.virginia.edu/catalog/libra-oa:2577>
- Ehlmann, B. L., & Edwards, C. S. (2014). Mineralogy of the Martian Surface. *Annual Review of Earth and Planetary Sciences*, *42*. doi: 10.1146/annurev-earth-060313-055024
- Encrenaz, T., DeWitt, C., Richter, M. J., Greathouse, T. K., Fouchet, T., Montmessin, F., ... Sagawa, H. (2018). New measurements of D/H on Mars using EXES aboard SOFIA. *Astronomy & Astrophysics*, *612*. doi:

10.1051/0004-6361/201732367

- Fedorova, A. A., Montmessin, F., Korablev, O., Luginin, M., Trokhimovsky, A., Belyaev, D. A., . . . Wilson, C. F. (2020). Stormy water on Mars: the behavior and saturation of atmospheric water during the dusty season. *Submitted to Science*, 9522. doi: 10.1126/science.aay9522
- Forget, F., Montmessin, F., Bertaux, J.-L., González-Galindo, F., Lebonnois, S., Quémerais, E., . . . López-Valverde, M. A. (2009). Density and temperatures of the upper Martian atmosphere measured by stellar occultations with Mars Express SPICAM. *Journal of Geophysical Research (Planets)*, 114. doi: 10.1029/2008JE003086
- Fouchet, T., & Lellouch, E. (1999). Vapor Pressure Isotope Fractionation Effects in Planetary Atmospheres: Application to Deuterium. *Icarus*, 144. doi: 10.1006/icar.1999.6264
- Gacesa, M., Zhang, P., & Kharchenko, V. (2012). Non-thermal escape of molecular hydrogen from Mars. *Geophysical Research Letters*, 39. doi: 10.1029/2012GL050904
- Geiss, J., & Reeves, H. (1981). Deuterium in the solar system. *Astronomy & Astrophysics*, 93.
- Heavens, N. G., Kleinböhl, A., Chaffin, M. S., et al. (2018). Hydrogen escape from Mars enhanced by deep convection in dust storms. *Nature Astronomy*, 2. doi: 10.1038/s41550-017-0353-4
- Hunten, D. M. (1973). The Escape of Light Gases from Planetary Atmospheres. *Journal of the Atmospheric Sciences*, 30. doi: 10.1016/0032-0633(82)90110-6
- Jakosky, B. M., Brain, D. A., Chaffin, M. S., et al. (2018). Loss of the Martian atmosphere to space: Present-day loss rates determined from MAVEN observations and integrated loss through time. *Icarus*. doi: 10.1016/j.icarus.2018.05.030
- Klingelhöfer, G., Morris, R. V., Bernhardt, B., Schröder, C., Rodionov, D. S., de Souza, P. A., . . . Arvidson, R. E. (2004). Jarosite and Hematite at Meridiani Planum from Opportunity's Mössbauer Spectrometer. *Science*, 306. doi: 10.1126/science.1104653
- Krasnopolsky, V. (1993). Photochemistry of the Martian Atmosphere (Mean Conditions). *Icarus*, 101. doi: 10.1006/icar.1993.1027
- Krasnopolsky, V. (2000). On the Deuterium Abundance on Mars and Some Related Problems. *Icarus*, 148. doi: 10.1006/icar.2000.6534
- Krasnopolsky, V., Bjoraker, G., Mumma, M., & Jennings, D. (1997). High-resolution spectroscopy of Mars at 3.7 and 8 μm : A sensitive search for H₂O₂, H₂CO, HCl, and CH₄, and detection of HDO. *Journal of Geophysical Research*, 102. doi: 10.1029/96JE03766
- Krasnopolsky, V. A. (2002). Mars' upper atmosphere and ionosphere at low, medium, and high solar activities: Implications for evolution of water. *Journal of Geophysical Research: Planets*, 107. doi: 10.1029/2001JE001809
- Krasnopolsky, V. A. (2010). Solar activity variations of thermospheric temperatures on Mars and a problem of CO in the lower atmosphere. *Icarus*, 207. doi: 10.1016/j.icarus.2009.12.036
- Krasnopolsky, V. A., & Feldman, P. D. (2001). Detection of molecular hydrogen in the atmosphere of Mars. *Science*, 294. doi: 10.1126/science.1065569
- Krasnopolsky, V. A., & Mumma, M. J. (1998). Detection of Atomic Deuterium in the Upper Atmosphere of Mars. *Science*, 280. doi: 10.1126/science.280.5369.1576
- Kurokawa, H., Sato, M., Ushioda, M., Matsuyama, T., Moriwaki, R., Dohm, J. M., & Usui, T. (2014). Evolution of water reservoirs on Mars: Constraints from hydrogen isotopes in martian meteorites. *Earth and Planetary Science Letters*, 394. doi: 10.1016/j.epsl.2014.03.027
- Lammer, H., Kolb, C., Penz, T., Amerstorfer, U. V., Biernat, H. K., & Bodiselitsch,

- B. (2003). Estimation of the past and present Martian water-ice reservoirs by isotopic constraints on exchange between the atmosphere and the surface. *International Journal of Astrobiology*, *2*. doi: 10.1017/S1473550403001605
- Laskar, J., Correia, A., Gastineau, M., Joutel, F., Levrard, B., & Robutel, P. (2004). Long term evolution and chaotic diffusion of the insolation quantities of Mars. *Icarus*, *170*. doi: 10.1016/J.ICARUS.2004.04.005
- Lasue, J., Mangold, N., Hauber, E., et al. (2013). Quantitative Assessments of the Martian Hydrosphere. *Space Science Reviews*, *174*. doi: 10.1007/s11214-012-9946-5
- Liu, S., & Donahue, T. (1976). The regulation of hydrogen and oxygen escape from Mars. *Icarus*, *28*. doi: 10.1016/0019-1035(76)90035-X
- Mahaffy, P. R., Webster, C. R., Stern, J. C., Brunner, A. E., Atreya, S. K., Conrad, P. G., ... Wray, J. J. (2015). The imprint of atmospheric evolution in the D/H of hesperian clay minerals on Mars. *Science*, *347*. doi: 10.1126/science.1260291
- Maltagliati, L. (2011). Evidence of Water Vapor in Excess of Saturation in the Atmosphere of Mars. *Science*, *333*. doi: 10.1126/science.1207957
- Manion, J. A., Huie, R. E., Levin, R. D., Burgess Jr., D. R., Orkin, V. L., Tsang, W., ... Frizzell, D. H. (2015). *NIST Chemical Kinetics Database*. Retrieved 2015-09, from <http://kinetics.nist.gov/>
- Marti, J., & Mauersberger, K. (1993). A Survey and New Measurements of Ice Vapor Pressure at Temperatures Between 170 and 250K. *Geophysical Research Letters*, *20*. doi: 10.1029/93GL00105
- Matta, M., Withers, P., & Mendillo, M. (2013). The composition of Mars' topside ionosphere: Effects of hydrogen. *Journal of Geophysical Research: Space Physics*, *118*. doi: 10.1002/jgra.50104
- McElroy, D., Walsh, C., Markwick, A. J., Cordiner, M. A., Smith, K., & Millar, T. J. (2013). *The UMIST database for Astrochemistry 2012*.
- McElroy, M. B., Kong, T. Y., & Yung, Y. L. (1977). Photochemistry and Evolution of Mars' Atmosphere: A Viking Perspective. *Journal of Geophysical Research*, *82*. doi: 10.1029/JS082i028p04379
- Millour, E., & Forget, F. (2018). *Mars Climate Database*. Retrieved from <http://www-mars.lmd.jussieu.fr/>
- Montmessin, F., Fouchet, T., & Forget, F. (2005). Modeling the annual cycle of HDO in the Martian atmosphere. *Journal of Geophysical Research E: Planets*, *110*. doi: 10.1029/2004JE002357
- Nair, H., Allen, M., Anbar, A. D., & Yung, Y. L. (1994). A Photochemical Model of the Martian Atmosphere. *Icarus*, *111*. doi: 10.1006/icar.1994.1137
- Nee, J. B., & Lee, L. C. (1984). Photoabsorption cross section of OD at 115-180 nm. *The Journal of Chemical Physics*, *81*. doi: 10.1063/1.448183
- Owen, T., Maillard, J. P., de Bergh, C., & Lutz, B. L. (1988). Deuterium on Mars: The Abundance of HDO and the Value of D/H. *Science (New York, N.Y.)*, *240*. doi: 10.1126/science.240.4860.1767
- Plaut, J. J., Picardi, G., Safaeinili, A., Ivanov, A. B., Milkovich, S. M., Cicchetti, A., ... Edenhofer, P. (2007). Subsurface Radar Sounding of the South Polar Layered Deposits of Mars. *Science*, *316*. doi: 10.1126/science.1139672
- Sander, S. P., Friedl, R. R., Golden, D. M., Kurylo, M. J., Moortgat, G. K., Wine, P. H., ... Orkin, V. L. (2011). Chemical Kinetics and Photochemical Data for Use in Atmospheric Studies Evaluation Number 15. *Cross Sections*. doi: 10.1002/kin.550171010
- Savijärvi, H., McConnochie, T. H., Harri, A. M., & Paton, M. (2019). Water vapor mixing ratios and air temperatures for three martian years from Curiosity. *Icarus*, *326*. doi: 10.1016/j.icarus.2019.03.020
- Seiff, A. (1982). Post-Viking models for the structure of the summer atmosphere of Mars. *Advances in Space Research*, *2*. doi: 10.1016/0273-1177(82)90102-8

- Shaposhnikov, D. S., Medvedev, A. S., Rodin, A. V., & Hartogh, P. (2019). Seasonal Water "Pump" in the Atmosphere of Mars: Vertical Transport to the Thermosphere. *Geophysical Research Letters*, *46*. doi: 10.1029/2019GL082839
- Smith, M. D. (2004). Interannual variability in TES atmospheric observations of Mars during 1999-2003. *Icarus*, *167*. doi: 10.1016/j.icarus.2003.09.010
- Smith, M. D., Wolff, M. J., Spanovich, N., Ghosh, A., Banfield, D., Christensen, P. R., ... Squyres, S. W. (2006). One Martian year of atmospheric observations using MER Mini-TES. *Journal of Geophysical Research E: Planets*, *111*. doi: 10.1029/2006JE002770
- Squyres, S. W., Grotzinger, J. P., Arvidson, R. E., Bell, J. F., Calvin, W., Christensen, P. R., ... Soderblom, L. A. (2004). In Situ Evidence for an Ancient Aqueous Environment at Meridiani Planum, Mars. *Science*, *306*. doi: 10.1126/science.1104559
- Stone, S. W., Yelle, R. V., Benna, M., Elrod, M. K., & Mahaffy, P. R. (2018). Thermal Structure of the Martian Upper Atmosphere From MAVEN NGIMS. *Journal of Geophysical Research: Planets*. doi: 10.1029/2018JE005559
- Thiemann, E. M. B., Eparvier, F. G., Bougher, S. W., Dominique, M., Andersson, L., Girazian, Z., ... Jakosky, B. M. (2018). Mars Thermospheric Variability Revealed by MAVEN EUVM Solar Occultations: Structure at Aphelion and Perihelion and Response to EUV Forcing. *Journal of Geophysical Research (Planets)*, *123*. doi: 10.1029/2018JE005550
- Trainer, M. G., Wong, M. H., McConnochie, T. H., Franz, H. B., Atreya, S. K., Conrad, P. G., ... Zorzano, M. P. (2019). Seasonal Variations in Atmospheric Composition as Measured in Gale Crater, Mars. *Journal of Geophysical Research: Planets*, *124*. doi: 10.1029/2019JE006175
- Usui, T., Alexander, C. M. O., Wang, J., Simon, J. I., & Jones, J. H. (2012). Evidence from Olivine-Hosted Melt Inclusions that the Martian Mantle has a Chondritic D/H Ratio and that Some Young Basalts have Assimilated Old Crust. In *Lunar and planetary science conference*.
- Vandaele, A. C., Korablev, O., Daerden, F., Aoki, S., Thomas, I. R., Altieri, F., ... others (2019). Martian dust storm impact on atmospheric H₂O and D/H observed by ExoMars Trace Gas Orbiter. *Nature*, *568*. doi: 10.1038/s41586-019-1097-3
- Vasavada, A. R., Piqueux, S., Lewis, K. W., Lemmon, M. T., & Smith, M. D. (2016). Thermophysical properties along Curiosity's traverse in Gale crater, Mars, derived from the REMS ground temperature sensor. *Icarus*, *284*. doi: 10.1016/j.icarus.2016.11.035
- Villanueva, G. L., Liuzzi, G., Crismani, M. M., et al. (2019). Strong seasonal and diurnal variability of water D/H on Mars as revealed with ExoMars/NOMAD. In *Epsc abstracts*. (EPSC-DPS2019-1471)
- Villanueva, G. L., Mumma, M. J., Novak, R. E., et al. (2015). Strong water isotopic anomalies in the martian atmosphere: Probing current and ancient reservoirs. *Science*, *348*. doi: 10.1126/science.aaa3630
- Wakelam, V., & Gratier, P. (2019). *Kinetic Database for Astrochemistry*. Retrieved from <http://kida.obs.u-bordeaux1.fr/contact.html>
- Woods, T. N., Chamberlin, P. C., Harder, J. W., Hock, R. A., Snow, M., Eparvier, F. G., ... Richard, E. C. (2019). *LISIRD (LASP Interactive Solar Irradiance Datacenter)*. Retrieved from <http://lasp.colorado.edu/lisird/>
- Wordsworth, R. D., Kerber, L., Pierrehumbert, R. T., Forget, F., & Head, J. W. (2015). Comparison of "warm and wet" and "cold and icy" scenarios for early Mars in a 3D climate model. *Journal of Geophysical Research: Planets*. doi: 10.1002/2015JE004787
- Yung, Y. L., & DeMore, W. B. (1998). *Photochemistry of Planetary Atmospheres*. Oxford University Press.
- Yung, Y. L., Wen, J.-S., Moses, J. I., Landry, B. M., Allen, M., & Hsu, K.-J. (1989).

- Hydrogen and deuterium loss from the terrestrial atmosphere: A quantitative assessment of nonthermal escape fluxes. *Journal of Geophysical Research*, 94.
- Yung, Y. L., Wen, J. S., Pinto, J. P., Allen, M., Pierce, K. K., & Paulson, S. (1988). HDO in the Martian atmosphere: Implications for the abundance of crustal water. *Icarus*, 76. doi: 10.1016/0019-1035(88)90147-9
- Zahnle, K., Haberle, R. M., Catling, D. C., & Kasting, J. F. (2008). Photochemical instability of the ancient Martian atmosphere. *Journal of Geophysical Research E: Planets*, 113. doi: 10.1029/2008JE003160
- Zuber, M. T., Smith, D. E., Solomon, S. C., Abshire, J. B., Afzal, R. S., Aharonson, O., . . . Duxbury, T. C. (1998). Observations of the North Polar Region of Mars from the Mars Orbiter Laser Altimeter. *Science*, 282. doi: 10.1126/science.282.5396.2053